

Ratiometric Fluorescence Monitoring of Antibody-Guided Drug Delivery to Cancer Cells

Dvir Poplinger, Maksym Bokan, Arkadi Hesin, Ebaston Thankarajan, Helena Tuchinsky, Gary Gellerman, and Leonid Patsenker*

Cite This: <https://doi.org/10.1021/acs.bioconjchem.1c00205>

Read Online

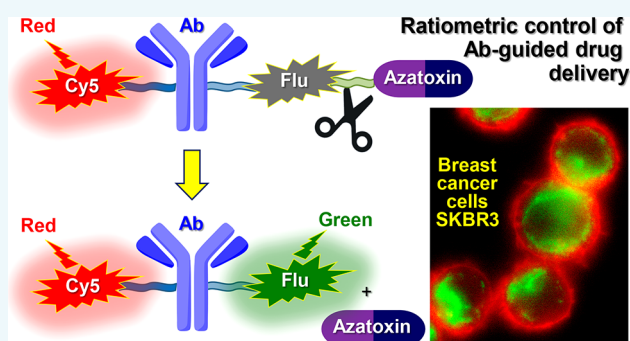
ACCESS |

Metrics & More

Article Recommendations

Supporting Information

ABSTRACT: Ratiometric measurements utilizing two independent fluorescence signals from a dual-dye molecular system help to improve the detection sensitivity and quantification of many analytical, bioanalytical, and pharmaceutical assays, including drug delivery monitoring. Nevertheless, these dual-dye conjugates have never been utilized for ratiometric monitoring of antibody (Ab)-guided targeted drug delivery (TDD). Here, we report for the first time on the new, dual-dye TDD system, Cy5s-Ab-Flu-Aza, comprising the switchable fluorescein-based dye (Flu) linked to the anticancer drug azatoxin (Aza), reference pentamethine cyanine dye (Cy5s), and Her2-specific humanized monoclonal Trastuzumab (Herceptin) antibody. The ability of ratiometric fluorescence monitoring of drug release was demonstrated with this model system *in vitro* in the example of the human breast cancer SKBR3 cell line overexpressing Her2 receptors. The proposed approach for designing ratiometric, antibody-guided TDD systems, where a “drug–switchable dye” conjugate and a reference dye are independently linked to an antibody, can be expanded to other drugs, dyes, and antibodies. Replacement of the green-emitting dye Flu, which was found not detectable *in vivo*, with a longer-wavelength (red or near-IR) switchable fluorophore should enable quantification of drug release in the body.



INTRODUCTION

Targeted drug delivery (TDD) systems, consisting of a drug or prodrug bound to a target-specific carrier¹ such as an antibody,^{2–4} peptide,^{5–9} nanoparticle,^{10–12} or extracellular matrix compounds,¹³ facilitate drug delivery, minimize side effects to normal cells and organs, and thereby help to improve the safety of treatment in clinics.^{14,15} TDD systems additionally equipped with a switchable fluorescent dye (SD) bound to the drug or prodrug through a cleavable linker (Figure 1a) provide real-time monitoring of drug distribution and

accumulation, as well as detection and diagnosis of abnormal cells.^{16,17} Upon the environment-mediated cleavage of the linker, the switchable dye becomes fluorescent or changes its emission wavelength, signaling the drug release. The fluorescence signal from the dye is, however, affected by the light absorption and scattering in the biological sample, in particular, in the body, and is also dependent on the instrumental setup.^{18,19} The dual-signal ratiometric fluorescence measurements utilizing a second, nonswitchable reference dye (RD, Figure 1b) provide internal calibration which eliminates these undesirable factors and improves the detection sensitivity and quantification.^{20–23}

Recently, a variety of dual-signal ratiometric drug delivery systems have been introduced and summarized in several reviews.^{16,24,25} As an example, the dual fluorescence drug delivery conjugate CDox containing no targeting carrier was developed, where the fluorescent anticancer drug doxorubicin (Dox) and the fluorescent coumarin dye (C) were conjugated

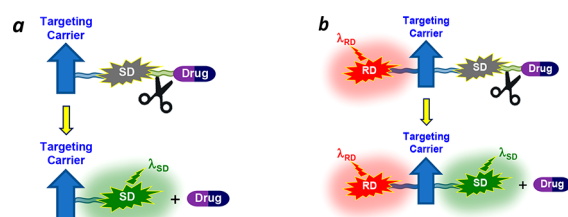


Figure 1. Targeted drug delivery (TDD) systems equipped with a switchable fluorescent dye (SD) to monitor drug release events (a) and a TDD system containing an additional nonswitchable reference dye (RD) enabling ratiometric fluorescence monitoring of drug delivery and drug release (b). SD and RD emit light at different wavelengths, λ_{SD} and λ_{RD} , respectively.

Received: April 21, 2021

Revised: May 27, 2021

to each other by a pH-responsive cleavable hydrazone linker.^{26,27} The resulting **CDox** conjugate is not fluorescent; although upon the **Dox** release, it exhibits dual turn-on signals with emission peaks at 595 and 488 nm, related to coumarin and **Dox**, respectively. The proposed dual-signal method cannot be utilized for the ratiometric measurements as both signals enhance simultaneously. This approach is also limited by the drug, which must be fluorescent.

A more general approach for the ratiometric drug delivery monitoring was realized using the dual fluorescent **amino-BODIPY** dye.²⁸ The model anticancer drugs derived from 2-phenyl-3-hydroxy-4(1*H*)-quinolinone were substituted by the thiol, hydroxy, or amino group and conjugated with the dye through a glutathione cleavable disulfide linker. The drug-conjugated dye absorbs at 510 nm, while in the free form, the absorption maximum is blue-shifted to 480 nm. Both the conjugated and free forms of the dye emit at the same wavelength. The obtained conjugates were tested in HeLa cells pretreated with glutathione for ratiometric monitoring of the drug release using the one emission and two excitation wavelengths. The developed drug delivery conjugate was unfortunately not supplied with a targeting carrier.

A single switchable dye, heptamethine cyanine **CyA**, containing a trigger hydroxyl group in the central cyclohexene moiety, was proposed for the dual-channel *in vivo* monitoring of an activatable prodrug delivery in thiol-triggered chemotherapy.²⁹ The anticancer drug camptothecin (**CPT**) was linked to the dye via a disulfide linker through a biodegradable carbonate moiety. The cleavage of the disulfide bond by endogenous glutathione activated the **CPT** and induced a remarkable fluorescence shift from 825 to 650 nm, thereby providing dual fluorescent channels to real-time monitoring of the prodrug distribution and activation *in vivo*, which was demonstrated in a mice model. This **CyA-CPT** conjugate was also not equipped with a targeting carrier.

A peptide-guided TDD system, utilizing a similar dual-signal heptamethine cyanine dye, **IRD**, was proposed for dual-channel monitoring of anticancer drug chlorambucil (**CLB**) delivery to the Panc-1 cancer cell line.⁸ The fluorescence maximum of this NIR dye (805 nm) was blue-shifted to 526 nm upon the drug release. Applications of heptamethine cyanine dyes of similar structure in TDD monitoring were reviewed elsewhere.³⁰

A ratiometric system utilizing FRET between NIR emitting **Cy5.SLP** and **Cy7.SLP** lipophilic cyanine dyes encapsulated in lipid nanocarriers was developed and employed for tumor quantification in living mice.³¹ This system can potentially be utilized for delivery of drugs encapsulated in the lipid nanocarriers.

Apart from what was stated above, to the best of our knowledge, dual-dye ratiometric TDD systems (covalent conjugates) based on a target-specific antibody have never been previously designed, although fluorescently labeled antibodies are widely utilized for diagnostic applications.^{32,33}

Recently, we reported on the synthesis of chemosensing **Drug-Flu-COOH** conjugates for fluorescence drug delivery monitoring.³⁴ Some of the reported conjugates comprised activatable fluorescein dye (**Flu**) bound to anticancer drugs amonafide, tubulizine, and curcumine through a hydrolytically cleavable acrylate ester linker. These conjugates were synthesized through a propiolic fluorescein derivative.

In this work, we decided to conjugate the same propiolic **Flu** precursor to another topoisomerase II-targeted anticancer drug

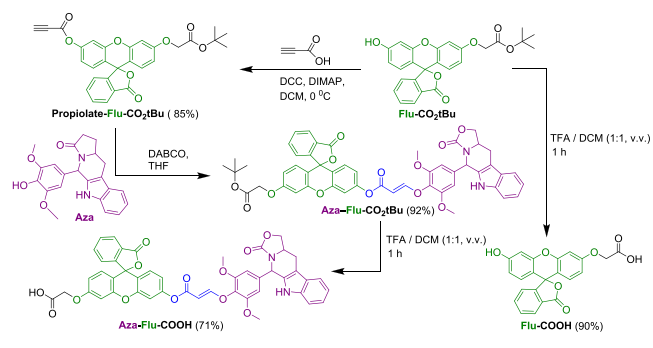
azatoxin (**Aza**)³⁵ to obtain **Aza-Flu-COOH**. In hydrolytic media, this conjugate has to release **Aza**, subsequently increasing the **Flu** emission signal, which indicates the drug release event. Furthermore, we utilize this **Aza-Flu-COOH** conjugate to create a model antibody-guided TDD system enabling ratiometric fluorescence monitoring of targeted drug delivery. To achieve this goal, **Aza-Flu-COOH** is linked to the recombinant monoclonal Ab Trastuzumab (**Herceptin**) fluorescently labeled with the red-emitting pentamethine cyanine dye **Cy5s**. The obtained dual-dye TDD system, **Cy5s-Ab-Flu-Aza**, is then tested for real-time ratiometric monitoring of targeted drug delivery of azatoxin to the SKBR3 cancer cell line. Several other model conjugates are also synthesized and tested as the control. Trastuzumab antibody (**Ab**) is specific to Her2 receptors overexpressed by the SKBR3 human breast cancer cell line.³⁶ This cell line is a useful model to screen for therapeutic agents targeting Her2 and to describe mechanisms of their resistance to Her2-targeted therapies.³⁷ It is noteworthy that SKBR3 cells display an epithelial morphology in tissue culture and are capable of forming poorly differentiated tumors in immunocompromised mice.³⁸

The combination of the targeting antibody trastuzumab and the drug azatoxin was chosen since this **Ab** targets many types of cancer that can be treated with azatoxin. Thus, apart from breast cancer, trastuzumab is also known to treat Her2 positive stomach (gastric),³⁹ colorectal,⁴⁰ and lung⁴¹ cancers, melanoma,⁴² and leukemia.^{43,44} At the same time, azatoxin, which serves as a model drug, is a cytotoxic agent that inhibits both tubulin and topoisomerase II. It is active against colorectal and lung cancer, melanoma, and leukemia, producing 50% growth inhibition (GI_{50}) at mean concentration of 0.13 μM .⁴⁵

RESULTS AND DISCUSSION

Synthesis. **Aza-Flu-COOH**, which is the key intermediate for the antibody-guided, dual-dye **Cy5s-Ab-Flu-Aza** conjugate, was synthesized according to the previously reported method³⁴ starting from fluorescein and azatoxin (**Aza**), as shown in **Scheme 1**. Briefly, dilithium salt of fluorescein (**1**), obtained

Scheme 1. Synthesis of **Aza-Flu-COOH** and **Flu-COOH**

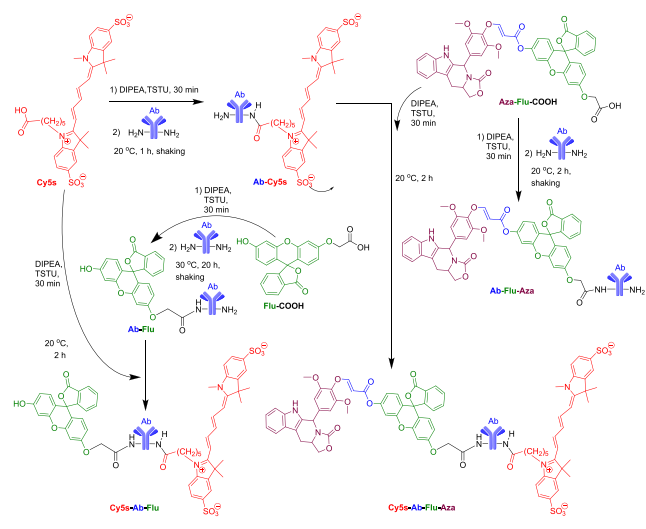


from the fluorescein by adding aqueous **LiOH**, was reacted with *tert*-butyl bromoacetate to form the monosubstituted fluorescein **Flu-CO₂tBu**. The last one was preactivated with **DCC** and **DMAP** in **DCM** and coupled with propiolic acid to give 3'-(2-(*tert*-butoxy)-2-oxoethoxy)-3-oxo-3*H*-spiro-[isobenzofuran-1,9'-xanthen]-6'-yl propiolate (**Propiolate-Flu-CO₂tBu**) in good yield. Then, **Propiolate-Flu-CO₂tBu** was coupled by Michael addition to **Aza** in the presence of **DABCO** in **THF** to form the **Aza-Flu-CO₂tBu** in high yield. The *tert*-butyl group in **Aza-Flu-CO₂tBu** was then removed by

TFA in DCM (1:1, v.v.), and the Aza-Flu-COOH was finally obtained in a 71% yield. Flu-COOH was synthesized from Flu-CO₂tBu in a 90% yield (Scheme 1), as described in the work.⁴⁶

Then, Ab-Cy5h, Ab-Cy5s, Ab-Flu, and Ab-Flu-Aza conjugates were obtained according to the common Ab coupling method⁴⁷ with Cy5h, Cy5s, Flu-COOH, and Aza-Flu-COOH, respectively, using the TSTU coupling reagent and lyophilized (Scheme 2). To determine the dye-to-antibody

Scheme 2. Synthesis of Cy5s-Ab-Flu-Aza, Ab-Flu, Ab-Flu-Aza, and Cy5s-Ab-Flu



ratio (DAR), the absorption spectra of the conjugates were measured in phosphate buffer pH 7.4 (Figure 2a and supplementary Figures S1–S3), and the DAR values were determined by using the peak absorbances of the dye and antibody and their extinction coefficients (see eq 1 in the Experimental Section). For Ab-Cy5h and Ab-Cy5s, the DARs were about 3.0, for Ab-Flu DAR ~ 2.4, and for Ab-Flu-Aza DAR ~ 1.0. The DAR ~ 3.0 for Ab-Cy5s is known to be an optimal value to avoid aggregation and provide the most intense emission signal.⁴⁸ The DAR values for all the conjugates synthesized in this work are shown in Table S1.

It was reported that the direct NHS-based coupling, which we applied in our work, allowed achieving the DAR ~ 6 for Cy5s⁴⁸ and even higher, in the order of DAR ~ 9,^{49,50} for some other dyes. It means that at least 3–6 free amino groups are still available in the antibody to bind the second dye (Flu-COOH) or drug–dye conjugate (Aza-Flu-COOH) to yield the Cy5s-Ab-Flu and Cy5s-Ab-Flu-Aza conjugates, respectively.

Cy5s-Ab-Flu-Aza, DAR(Cy5s) ~ 3.0 and DAR(Flu) ~ 1.0, was synthesized from Ab-Cy5s according to the same coupling procedure: the carboxylic group in Aza-Flu-COOH was first activated and then coupled to the amino group of the Cy5s labeled antibody (Scheme 2). The DAR ~ 3.0 measured for the starting Ab-Cy5s conjugate remained unchanged in the resulted Cy5s-Ab-Flu-Aza.

The dual-fluorescent Cy5s-Ab-Flu conjugate, DAR(Cy5s) ~ 1.5 and DAR(Flu) ~ 2.4, was also synthesized for comparison from Ab-Flu and Cy5s by the same method.

All the conjugates were purified by gel permeation chromatography (Sephadex G50) and lyophilized. Due to unstable emission intensity of Ab-Cy5h (bearing hydrophobic dye) over time (see below), we decided to focus only on the dual-dye Cy5s-Ab-Flu-Aza conjugate comprising the hydrophilic dye Cy5s.

Spectral Properties. The absorption and emission spectra of Ab-Flu (Figure S1), Ab-Flu-Aza (Figure S1), Ab-Cy5h (Figure S2), Ab-Cy5s (Figure S2), Cy5s-Ab-Flu (Figure 2a), and Cy5s-Ab-Flu-Aza (Figure 2a) were measured in phosphate buffer pH 7.4. While Ab-Flu-Aza does not absorb at ~480 nm and does not fluoresce (Flu exists in the “off” form), Ab-Flu has a green fluorescence with maximum at ~519 nm.

Cy5h and Cy5s in both free and Ab-conjugated form emit at about 670 nm (Figure S2), free Flu-COOH emission is at ~519 nm, while the drug-conjugated Aza-Flu-COOH shows no detectable absorption and fluorescence. Therefore, the freshly prepared sample of Cy5s-Ab-Flu-Aza exhibits only the absorption and emission related to Cy5s (Figure 2a), while the Cy5s-Ab-Flu conjugate shows both red Cy5s and green Flu (“on”) spectral bands (Figure 2a).

The absorption and emission spectra of cyanine dyes contain a vibration mode that can be seen as a shoulder on the slope of the spectral curves.⁵¹ For Cy5h and Cy5s, this mode can be

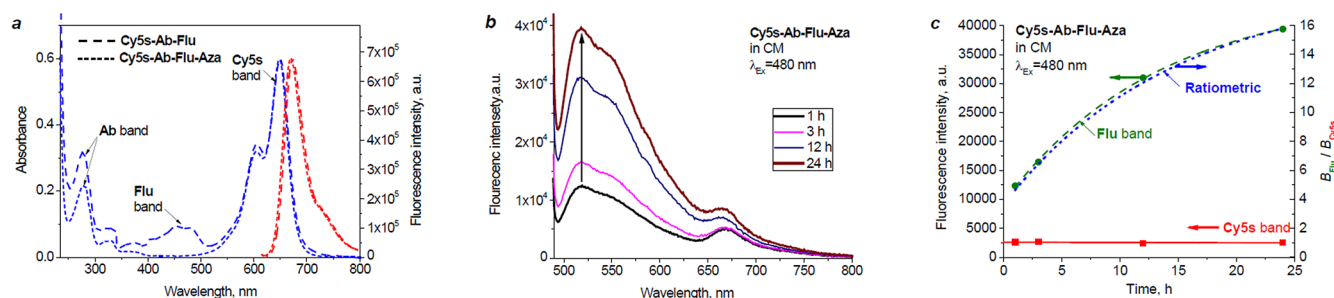


Figure 2. (a) Absorption and emission spectra of Cy5s-Ab-Flu, DAR(Cy5s) ~ 1.5, and DAR(Flu) ~ 2.4 (dashed line) and Cy5s-Ab-Flu-Aza, DAR(Cy5s) ~ 3.0, and DAR(Flu) ~ 1.0 (dotted line) measured in phosphate buffer pH 7.4. $\lambda^* = 610$ nm. There is no absorption for Cy5s-Ab-Flu-Aza at 480 nm because Flu exists in the “off” form. This conjugate exhibits, therefore, no detectable fluorescence when excited at $\lambda^* = 480$ nm. (b) Time-dependent emission spectra ($\lambda^* = 480$ nm) and (c) the FRET efficiency over time estimated by the intensity of the Cy5s emission band at 670 nm (solid line) for Cy5s-Ab-Flu-Aza, DAR(Cy5s) ~ 3.0, and DAR(Flu) ~ 1.0 upon the drug release initiated by esterase containing RPMI cell culture media (CM). The change in the Flu signal and the ratiometric curve are shown with dashed and dotted lines, respectively, with incubation at 37 °C. The spectra were recorded at room temperature. To calculate the intensity of each Cy5s band, the contribution of the Flu band was taken into account.

found in the absorption spectrum at about 600 nm (Figure S2). Aggregation of cyanines is known to produce a new band, which is located in the same spectral region as the vibration mode.⁵² Therefore, the ratio R_{aggr} between the absorbances of the aggregated form (~ 600 nm) and free dye (~ 650 nm) can be used to characterize the dye aggregation ability. In addition, aggregation violates the mirror symmetry between the absorption and emission bands. It can be seen, therefore, that Cy5h ($R_{\text{aggr}} \sim 0.78$) compared to Cy5s ($R_{\text{aggr}} \sim 0.54$) strongly aggregates on the antibody at about the same DAR ~ 3.0 (Figure S2). Aggregation of dyes is known to decrease the brightness^{47,53,54} and increase the probability of nonspecific binding.^{55,56} As a result of the aggregation, the fluorescence intensity of Ab-Cy5h is about 7-fold reduced compared to Ab-Cy5s.

The shape of the Cy5s absorption band and the R_{aggr} values for the Ab-Cy5s, Cy5s-Ab-Flu-Aza, and Cy5s-Ab-Flu conjugates are about the same ($R_{\text{aggr}} \sim 0.54$), which indicates that the conjugation of Ab-Cy5s with Aza-Flu-COOH and Flu-COOH does not affect the Cy5s aggregation degree.

Surprisingly, binding of Aza-Flu-COOH to the Ab-Cy5s (DAR ~ 3.0) conjugate to yield Cy5s-Ab-Flu-Aza results in about a 5.6-fold decrease of the Cy5s emission (Figure S3). Because Aza-Flu-COOH does not affect the Cy5s aggregation on the antibody, this decrease is connected, more likely, with the interaction of these two chromophores on the antibody.

In the Cy5s-Ab-Flu-Aza conjugate, upon the acrylic ester linker cleavage, which is accompanied by the drug release, the spectral bands related to the Flu absorption and emission arise. It is important to note that the emission spectrum of the resulting conjugate Cy5s-Ab-Flu consists of the two bands, the Flu band at ~ 519 nm and the Cy5s band at ~ 670 nm (Figure 2b), which is similar to the Cy5s-Ab-Flu conjugate directly synthesized according to Scheme 2. The Ab-Cy5s conjugate does not show any detectable red fluorescence when excited at $\lambda^* = 480$ nm, and therefore, the Cy5s fluorescence for the Cy5s-Ab-Flu conjugate at $\lambda^* = 480$ nm can be attributed only to the FRET from the Flu ("on" form) to Cy5s that is located on the same Ab molecule. We investigated the effect of drug release in the Cy5s-Ab-Flu-Aza conjugate on the FRET efficiency that was estimated as the change of the Cy5s emission intensity over time, when excited at 480 nm (Figure 2c). The drug release was activated by the esterase containing RPMI cell culture medium at 37 °C, as described in the work.⁹ The FRET was found to be almost independent of the number of the released drug molecules. This is the anticipated result because the synthesized conjugate contains, in average, only one Flu-Aza, and therefore, the drug release in each conjugate molecule does not change the distance between the Flu and Cy5s fluorophores.

Interaction of Ab-Flu-Aza, Ab-Cy5h, and Ab-Cy5s Conjugates with the SKBR3 Cell Line. First, we verified that the synthesized Cy5s-Ab-Flu, Ab-Flu-Aza, and Cy5s-Ab-Flu-Aza conjugates provide selective delivery to Her2 positive SKBR3 cancerous cells. For this, specific staining of SKBR3 cells was compared to those for a control—MCF 10A nontumorigenic epithelial cell line with an undetectable level of Her2 receptors. In our experiments, SKBR3 and MCF 10A cells were exposed to the investigated conjugates (10 μM) for 30 min, washed with phenol red-free complete RPMI-1640 medium, and resuspended in this medium, and microscopic images were taken over time in both the transmitted light (bright field) and fluorescence mode. The green and red

emission channels (FITC and Cy5 cubes, respectively) were utilized to detect the Flu and Cy5 signals, respectively. In this experiment, we confirmed that the Ab-guided conjugates specifically stain Her2 positive SKBR3 cell lines but not Her2 negative MCF 10A cells (Figure S4).

Then, we investigated the interaction of the Ab-Flu-Aza, Ab-Cy5h, and Ab-Cy5s conjugates with the SKBR3 cell line. The total brightness for each image was quantified as the integrated density and represented as a graph over time (Figure 3a–c).

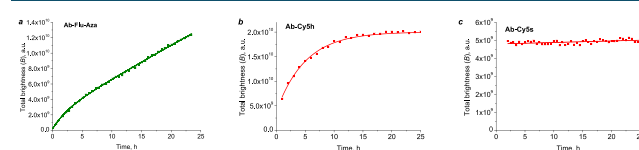
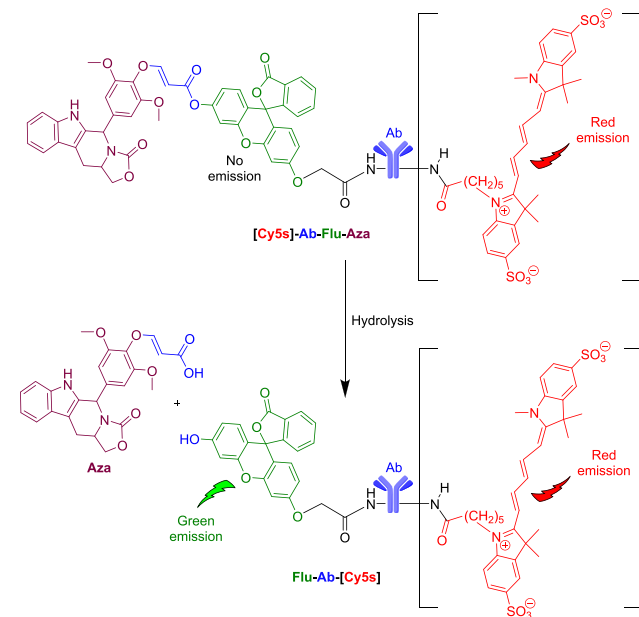


Figure 3. Time-dependent total brightness (B) of the SKBR3 cell line preliminarily treated for 30 min at 37 °C with the Ab-Flu-Aza (a), Ab-Cy5h (b), and Ab-Cy5s (c) conjugates. The Flu and Cy5h signals show a noticeable increase, while the Cy5s signal remains almost unchanged.

As anticipated, due to enzyme-triggered drug release from the Ab-Flu-Aza conjugate (Scheme 3), the emission signal of

Scheme 3. Drug Release from the Aza-Flu–Ab and Cy5s–Ab-Flu-Aza Conjugates



Flu exhibits a dramatic increase (Figure 3a), while the signal for the Ab-Cy5s conjugate remains almost unchanged (Figure 3c). At the same time, Ab-Cy5h compared to Ab-Cy5s surprisingly demonstrates an approximately 3.4-fold fluorescence increase (Figure 3b). This effect is more likely connected with sensitivity of this hydrophobic dye to the environment polarity. In contrast to the hydrophilic dye Cy5s, the Cy5h emission intensity substantially increases in lower-polar media, which can be the reason for the observed fluorescence increase in cells. Because the emission intensity of Cy5h changes substantially over time, this dye cannot be employed as the reference fluorophore for ratiometric measurements. We focused, therefore, as stated above, on the Cy5s-Ab-Flu-Aza

conjugate comprising the hydrophilic dye Cy5s. Importantly, the fluorescence intensity of the separately prepared Flu-Ab conjugate does not change during 24 h when interacting with SKBR3 cells, which suggests that the fluorescence increase for Ab-Flu-Aza occurs due to the drug release and not because of the change in the polarity.

Fluorescence TDD Monitoring in Cells. The Cy5s-Ab-Flu-Aza dual-dye conjugate was tested in the fluorescence intensity-based and ratiometric monitoring of targeted drug delivery. The experiment including SKBR3 cell preparation and treatment with the conjugate was carried out in the same way as for the single-dye conjugates, while the imaging was performed in both green and red channels simultaneously (Figure 4). As expected, the brightness of cells in the red

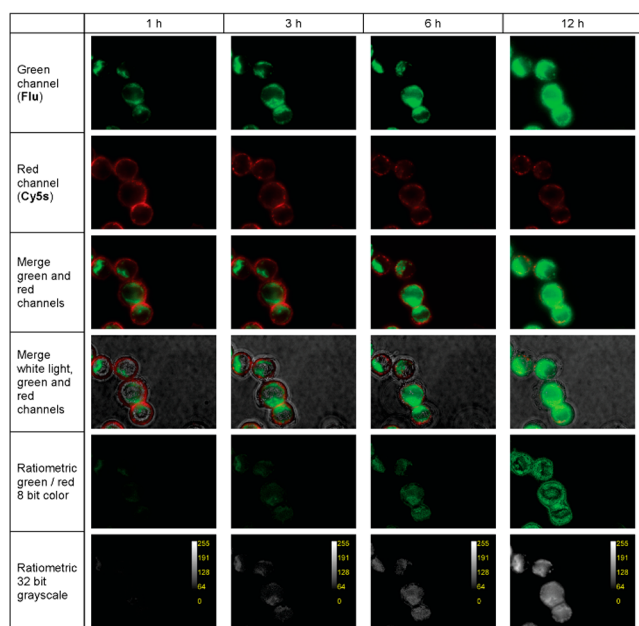


Figure 4. Time-dependent microscopic images of SKBR3 cells stained with Cy5s-Ab-Flu-Aza: fluorescence green and red channels, their overlays, overlay with white (bright field) light, and ratiometric (green/red) images obtained in the RGB and grayscale mode (supplied with the scale bar for fluorescence intensity in arbitrary units). SKBR3 cells were exposed to 10 μ M of the conjugate in PBS for 30 min and washed with PBS, and microscopic images were taken over time in both the bright field and fluorescence mode. The green and red emission channels were used to detect the Flu and Cy5s signals, respectively.

channel (Cy5s) remains almost constant, while the fluorescence signal in the green channel (Flu) significantly increases over time (by a factor of ~ 5 during 12 h and continues to increase after this period), indicating the drug release (Figure 5).

Based on the Cy5s-Ab-Flu-Aza fluorescence intensity profiles, the ratiometric curve was obtained as the ratio between the green and red signals (Figure 5, right axis). The half-life ($\tau_{1/2}$) of drug release obtained from both intensity-based and ratiometric profiles, fitted by a second-order exponential function, is about the same, in the order of $\tau_{1/2} \sim 4.0 \pm 0.5$ h. Compared to the brightness profiles, the ratiometric curve can be utilized to calculate the drug release degree independently of the sample and instrumental setup.^{20–23}

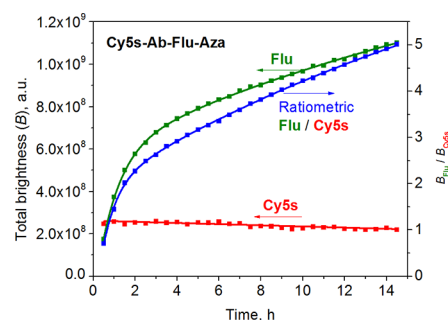


Figure 5. Time-dependent total brightness (B) obtained in the green (Flu) and red (Cy5s) channels (left axis) for the SKBR3 cell line preliminarily treated with Cy5s-Ab-Flu-Aza (37 $^{\circ}$ C, 30 min) and the ratiometric curve (right axis) obtained as the ratio between the brightnesses in the green (B_{Flu}) and in the red (B_{Cy5s}) channels.

Investigation of Cy5s-Ab-Flu-Aza in the Mice Model.

In the next step, we investigated the developed Cy5s-Ab-Flu-Aza conjugate for fluorescence monitoring of targeted drug delivery to the tumor in the mice model. As a control, we utilized Ab-Flu, constantly fluorescent in the green region, and Cy5s-Ab-Flu, constantly fluorescent in both green and red spectral regions. Six-week-old athymic nude mice ($n = 9$) were subcutaneously inoculated with SKBR3 cells, and tumors established over time. In 14 days, the Cy5s-Ab-Flu-Aza conjugate (100 μ L of 0.5 mg/mL solution in PBS) was injected iv (tail) in a group of six mice. Then, the white light and fluorescence images in the green and red channels were taken over time (Figure 6) for the tumor-bearing mice: (i)

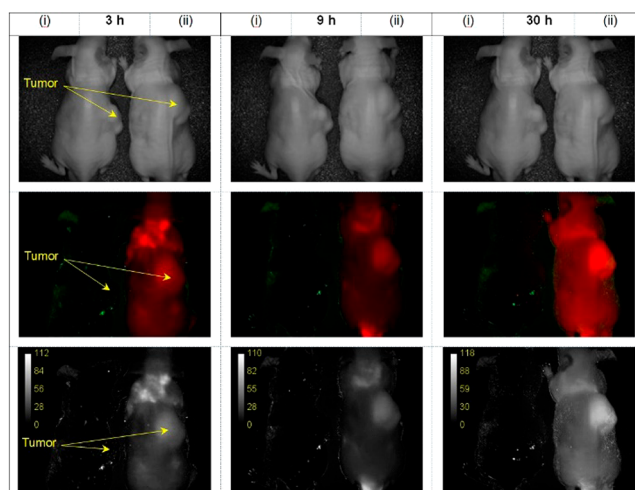


Figure 6. Normal-light images (top row), overlay of fluorescence images of mice obtained in the red and green channels (middle row), and grayscale images with the scale bars for fluorescence intensity (in arbitrary units) (bottom row): (i) mouse not administered with Cy5s-Ab-Flu-Aza and (ii) mouse administered with Cy5s-Ab-Flu-Aza.

naïve group (left) and (ii) injected with the Cy5s-Ab-Flu-Aza conjugate (right). As a control, the same experiment was performed with Ab-Flu and Cy5s-Ab-Flu conjugates (Figures S5 and S6). Each experiment was carried out in triplicate, and in each experiment, a naïve, tumor-bearing, and nonconjugate-administering mouse was used as a reference to compensate for the background autofluorescence.

We found that the green signal of Ab-Flu and Cy5s-Ab-Flu is not detectable in the body (Figures S5 and S6), which is

because of insufficient penetration of the blue excitation light and the green emission light through the skin but also due to the green autofluorescence of mice interfering with fluorescence measurements. Therefore, the increasing fluorescence of **Flu**, which was observed *in vitro* in SKBR3 cells stained with the **Cy5s-Ab-Flu-Aza** conjugate, was not detectable in the mice model (Figure 6). At the same time, the increasing red signal showing increasing accumulation of the conjugate in tumor compared to other organs was easily detected (Figures 6 and S7).

It worth mentioning that there are several publications asserting that the fluorescein-based dyes such as FITC, which contain both unsubstituted hydroxyl groups, do not provide a sufficient signal for detection in the body.^{57–60} The brightness (B) of FITC, estimated as the extinction coefficient ($\epsilon = 76,900 \text{ M}^{-1} \text{ cm}^{-1}$) multiplied by the fluorescence quantum yield ($\Phi_F = 0.93$), is $B = 71,500 \text{ M}^{-1} \text{ cm}^{-1}$ (when measured in phosphate buffer pH 7.4). At the same time, the brightness of **Flu** ("on" form, where only one hydroxyl group is protected as in the **Ab-Flu** and **Cy5s-Ab-Flu**) is $B = 8,540 \text{ M}^{-1} \text{ cm}^{-1}$ ($\epsilon = 24,400 \text{ M}^{-1} \text{ cm}^{-1}$, $\Phi_F = 0.35$),³⁴ which is as much as 8 times less than that for FITC. It becomes clear, therefore, that the **Flu** signal cannot be detected in the body and that the developed **Cy5s-Ab-Flu-Aza** system is suitable only for the ratiometric measurements *in vitro*.

After 30 h from the **Cy5s-Ab-Flu-Aza** conjugate injection, the organs (kidneys, spleen, lung, heart, and liver) and tumor of a group of (i) three nonadministered control mice and (ii) three conjugate-administered mice were resected and imaged (Figure 7). From a group of three other mice, the organs were taken for imaging in 6 days after the **Cy5s-Ab-Flu-Aza** injection (Figure S7).

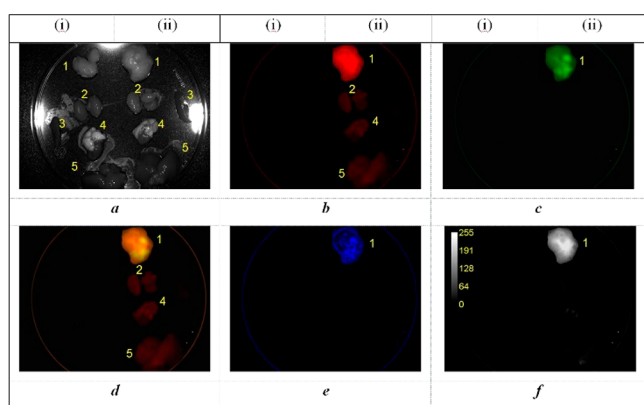


Figure 7. Normal-light (a) and fluorescence images of mice organs in the red (b) and green (c) channels, their overlay (d), and the ratiometric images (green divided by red) obtained in the RGB (e) and grayscale mode (supplied with the scale bar for fluorescence intensity in arbitrary units) (f): (i) mouse not administered with **Cy5s-Ab-Flu-Aza** and (ii) mouse administered with **Cy5s-Ab-Flu-Aza**. The organs were taken in 30 h after the **Cy5s-Ab-Flu-Aza** administration: 1—tumor; 2—kidneys; 3—spleen; 4—heart; 5—liver.

The images were recorded in the normal-light (Figure 7a) and in the fluorescence red (Figure 7b) and green (Figure 7c) modes. It can be seen that the tumor and organs of a representative mouse (i) not administered with **Cy5s-Ab-Flu-Aza** do not exhibit any detectable fluorescence. The tumor of the **Cy5s-Ab-Flu-Aza**-administered mouse (ii) shows a bright red emission (**Cy5s**), while the fluorescence of kidneys, lung,

heart, and liver is about 6-fold dimmer; emission of spleen is not detectable (Figure 7b). The tumor also possesses a clear green fluorescence of **Flu** (Figure 7c). Other investigated organs do not exhibit green fluorescence at the same imaging settings, which indicates preferable drug release in the tumor. Remarkably, the green signal has a slightly different brightness distribution than the red one. It could be associated with the fact that the release of drug is not homogeneous due to various cell subpopulations (so-called intratumor heterogeneity⁶¹) suggesting an unequal hydrolytic activity.^{62–64} Figure 7d shows an overlay of the red and green channels, while Figure 7e,f represents the ratiometric images (the time-dependent green signal divided by the reference red signal) obtained in the RGB and grayscale mode, respectively.

For the **Flu-Aza**- and **Cy5s-Ab-Flu**-administered mice, the green signal of the constantly fluorescent **Flu** is also detectable in the resected tumor but not *in vivo* (Figures S5 and S6). In addition, **Cy5s-Ab-Flu** produces an intense red signal well-recognized in live mice.

Since the ratiometric measurements failed in live mice because of the nondetectable green signal, we demonstrated the advantages of this method in the resected organs. The tumors of three mice were taken in 6 days after the **Cy5s-Ab-Flu-Aza** injection, and the fluorescence images were obtained in the red and green channels. Then, the ratios between the green and red intensities were calculated. The obtained data demonstrate that the green and red signals from the tumors can be noticeably different, while the ratio between them remains almost constant (Figure 8), which makes the ratiometric method independent of the sample.

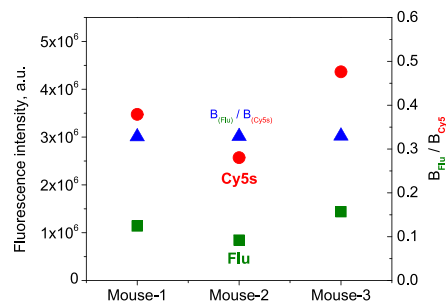


Figure 8. Fluorescence intensities of three resected mice tumors obtained in the green (**Flu**, squares) and red (**Cy5s**, circles) channels (left axis) and their ratios ($B_{\text{Flu}}/B_{\text{Cy5s}}$, triangles) for mice treated with **Cy5s-Ab-Flu-Aza**. The tumors were resected in 6 days after the conjugate administering.

CONCLUSION

In summary, we report on the synthesis of the novel, antibody-guided, dual-dye system, **Cy5s-Ab-Flu-Aza**, comprising the switchable fluorescein dye **Flu** conjugated to the anticancer drug azatoxin (**Aza**), reference dye **Cy5s**, and Her2-specific humanized monoclonal Trastuzumab (Herceptin) antibody for selective delivery to Her2 positive cancerous cells. A ratiometric fluorescence monitoring of drug release by using this system was demonstrated *in vitro* in the example of the SKBR3 cell line overexpressing Her2 receptors. Our model **Cy5s-Ab-Flu-Aza** system is applicable for the intensity-based monitoring of drug distribution and accumulation *in vitro* and *in vivo* and ratiometric measurements of drug release *in vitro*. Obviously, the proposed approach, where a drug is bound

through a switchable fluorophore to an antibody labeled with a permanently emitting reference dye, can be utilized to develop a ratiometric system with different drugs, fluorophores, and antibodies. Replacing the green, fluorescein-based fluorophore in this system with another red or near-IR emitting switchable dye should enable ratiometric quantification of drug release *in vivo*. Such research is currently under evaluation in our lab.

EXPERIMENTAL SECTION

General. HATU and DCC were purchased from Tzamal d-Chem Laboratories (Israel). All culture media and media supplements were obtained from Biological Industries (Israel). Solvents were from Bio-Lab Israel. All other chemicals were supplied by Alfa Aesar Israel and Sigma–Aldrich.

^1H and ^{13}C NMR spectra were measured by using a 400 MHz Bruker Avance III HD (^1H 400 MHz and ^{13}C 100 MHz) spectrometer in CDCl_3 using TMS as an internal standard. The probe was equipped with Z-axis gradients coils.

Mass spectra were measured in the positive and negative modes with a Waters Micromass Quattro micro instrument, which was equipped with an electrospray ionization source with Waters 2795 and 996 PDA detectors or an Auto flex III smart-beam (MALDI, Bruker).

LCMS analyses were performed on an Agilent Technologies 1260 Infinity (LC) 6120 quadruple (MS), column Agilent SB-C18, 1.8 mm, 2.1×50 mm, column temperature 50°C , eluent water–acetonitrile (ACN) that contained 0.1% of formic acid.

HPLC purifications were carried out on an ECOM preparative system, with dual UV detection at 254 and 230 nm. A Phenomenex Gemini 10 mm RP18 110 Å, LC 250 \times 21.2 mm column was used. The column was kept at RT: eluents A (0.1% TFA in water) and B (0.1% TFA in ACN). A typical elution was a gradient from 100% A to 100% B over 35 min at a flow rate of 25 mL/min.

Chemical reactions were monitored by TLC (silica gel 60 F-254, Merck) and LCMS. The purities of the dyes and conjugates were determined by LCMS.

The Ab conjugates were purified by Sephadex G50 gel permeation chromatography.

Synthesis. 3'-(2-(*tert*-Butoxy)-2-oxoethoxy)-3-oxo-3H-spiro[isobenzofuran-1,9'-xanthen]-6'-yl propiolate (**Propiolate-Flu-CO₂tBu**) was synthesized according to the procedure.³⁴

Flu-CO₂tBu (300 mg, 0.672 mmol) obtained as described in ref 34 and propiolic acid (42 μL , 0.672 mmol) were dissolved in dry DCM under nitrogen and cooled in a dry ice bath. Then, *N,N'*-dicyclohexylcarbodiimide (DCC) (166 mg, 0.804 mmol) and 4-dimethylaminopyridine (DMAP) (2 mg, 0.016 mmol) predissolved in DCM were added dropwise to this mixture. The reaction mixture was stirred for 40 min at 0°C , filtered, and solvent evaporated, and the product was purified on a preparative HPLC to give **Propiolate-Flu-CO₂tBu** (260 mg, 85%).

(E)-3'-(2-(*tert*-Butoxy)-2-oxoethoxy)-3-oxo-3H-spiro[isobenzofuran-1,9'-xanthen]-6'-yl 3-(2,6-Dimethoxy-4-(3-oxo-1,3,5,6,11,11a-hexahydrooxazolo[3',4':1,6]-pyrido[3,4-*b*]indol-5-yl)phenoxy)acrylate (Aza-Flu-CO₂tBu**). Azatoxin (**Aza**, 200 mg, 0.53 mmol) and DABCO (6 mg, 0.053 mmol) were dissolved in THF (10 mL) and stirred for 30 min at RT. **Propiolate-Flu-CO₂tBu** (264.2 mg, 0.53 mmol) dissolved in 5 mL of THF was added dropwise, followed by overnight stirring. After completion of the reaction, the solvent was evaporated, and the product was**

column purified (silica gel, hexane–ethyl acetate (2:1, v/v) to give **Aza-Flu-CO₂tBu** (428.5 mg, 92%) as a red oil. ^1H NMR (400 MHz, CDCl_3) δ ppm: 8.14 (s, 1 H), 8.02 (d, $J = 7.46$ Hz, 1 H), 7.83 (d, $J = 12.23$ Hz, 1 H), 7.59–7.72 (m, 2 H), 7.55 (d, $J = 7.70$ Hz, 1 H), 7.35 (d, $J = 7.95$ Hz, 1 H), 7.13–7.26 (m, 3 H), 7.09 (t, $J = 1.90$ Hz, 1 H), 6.58–6.83 (m, 7 H), 6.06 (s, 1 H), 5.45 (d, $J = 12.23$ Hz, 1 H), 4.54 (s, 2 H), 4.61 (t, $J = 8.31$ Hz, 1 H), 4.14–4.31 (m, 2 H), 3.76 (s, 6 H), 3.20 (dd, $J = 14.98$, 4.58 Hz, 1 H), 2.85 (ddd, $J = 14.95$, 10.55, 1.41 Hz, 1 H), 1.50 (s, 9 H). ^{13}C NMR (100 MHz, CDCl_3) δ ppm: 169.23, 167.37, 165.19, 163.81, 159.63, 156.83, 152.88, 152.20 (2 \times C), 152.12, 151.96, 151.74, 137.92, 136.66, 135.10, 132.51, 129.84, 129.16 (2 \times C), 128.87, 126.42, 126.16, 125.03, 124.06, 122.85, 118.29, 117.66, 112.01 (2 \times C), 111.85, 110.43, 108.81 (2 \times C), 105.19, 101.86, 98.36, 82.75, 82.33, 68.74, 67.91, 65.73, 56.42, 53.56 (2 \times C), 28.02, 27.10. LCMS: $R_f = 11.789$ min (254 nm, gradient 5–100% AcN– H_2O + 0.1% FA), MS: Calc.: (M)⁺ 878.3; Found: (M)⁺ 878.9.

(E)-2-((3'-(3-(2,6-Dimethoxy-4-(3-oxo-1,3,5,6,11,11a-hexahydrooxazolo[3',4':1,6]-pyrido[3,4-*b*]indol-5-yl)phenoxy)acryloyloxy)-3-oxo-3H-spiro[isobenzofuran-1,9'-xanthen]-6'-yl)oxy)acetic Acid (Aza-Flu-COOH**). **Aza-Flu-CO₂tBu** (100 mg, 0.11 mmol) was treated with TFA in DCM (1:1, v/v) at 0 – 5°C for 1 h. The solvent was evaporated under N_2 stream, and the residue was purified on a preparative HPLC and lyophilized to give **Aza-Flu-COOH** (64.5 mg, 71.3%) as a red powder. ^1H NMR (400 MHz, CDCl_3) δ ppm: 7.99–8.05 (m, 1 H), 7.97 (s, 1 H), 7.82 (dd, $J = 12.23$, 0.73 Hz, 1 H), 7.59–7.71 (m, 2 H), 7.55 (d, $J = 7.70$ Hz, 1 H), 7.31–7.37 (m, 1 H), 7.12–7.25 (m, 3 H), 7.08 (t, $J = 2.14$ Hz, 1 H), 6.60–6.84 (m, 7 H), 6.07 (s, 1 H), 5.45 (dd, $J = 12.23$, 0.86 Hz, 1 H), 4.70 (s, 2 H), 4.61 (t, $J = 8.38$ Hz, 1 H), 4.15–4.34 (m, 2 H), 3.70–3.81 (m, 6 H), 3.21 (dd, $J = 14.98$, 4.58 Hz, 1 H), 2.88 (ddd, $J = 15.01$, 10.55, 1.47 Hz, 1 H). ^{13}C NMR (100 MHz, CDCl_3) δ ppm: 168.30, 164.29, 162.92, 158.13, 156.00, 151.85 (3 \times C), 151.2 (2 \times C), 150.69, 136.82, 135.67, 134.20, 131.68, 128.94, 128.54, 128.49, 128.42, 127.90, 125.40, 125.18, 124.14, 121.98, 119.12, 117.34, 116.82, 115.34, 111.42 (2 \times C), 111.03, 110.37, 109.48 (2 \times C), 107.92, 100.95, 97.34, 81.27, 63.79, 58.52, 55.56, 55.50, 52.63, 29.02. LCMS: $R_f = 10.784$ min (254 nm, gradient 5–100% AcN– H_2O + 0.1% FA), MS: Calc.: (M)⁺ 822.1; Found: ($\text{M} + \text{H}$)⁺ 823.2, ($\text{M} + 2\text{H}$)⁺ 824.2. HRMS-ESI (+) calculated for $\text{C}_{46}\text{H}_{34}\text{N}_2\text{O}_{13}$, 822.2061; found 823.2237 (86%) [$\text{M} + \text{H}$]⁺, 845.2032 (18%) [$\text{M} + \text{Na}$].**

Ab-Flu-Aza (DAR ~ 1.0), Ab-Cy5h (DAR ~ 3.0), and Ab-Cy5s (DAR ~ 3.0). Dye **Cy5h**, **Cy5s**, or conjugate **Aza-Flu-COOH** (1 mg) was dissolved in DMF (1 mL), and then TSTU (2.5 mg, 8.3 μmol) and DIPEA (1.3 μL) were added. The reaction mixture was stirred for 30 min at 20°C . A stock solution (24 μL) of Trastuzumab (Herceptin antibody) (Ab, 21 mg/mL) was added to phosphate buffer pH 7.4 (PB, 220 μL). An aliquot of preactivated **Cy5h** or **Cy5s** or **Aza-Flu-COOH** (25 μL) was added to the Ab solution and stirred for 1–2 h at 20°C . The **Ab-Cy5h**, **Ab-Cy5s**, and **Ab-Flu-Aza** conjugates were separated from the unbound dyes by gel permeation chromatography (Sephadex G50). The first fraction containing the **Ab-Cy5h**, **Ab-Cy5s**, or **Ab-Flu-Aza** conjugate was collected. A sugar cryoprotectant (5 μL aliquot of 100 mg/mL solution) was then added to the Ab conjugate solution and lyophilized.

Ab-Flu (DAR ~ 2.4). Dye **Flu** (1 mg) was dissolved in DMF (0.25 mL), and then TSTU (5 mg, 16.6 μmol) and

DIPEA (5 μ L) were added. The reaction mixture was stirred for 30 min at 30 °C. A stock solution (94 μ L) of Trastuzumab Ab (21 mg/mL) was added to borate buffer pH 8.3 (0.416 mL). An aliquot of preactivated Flu (52 μ L) was added to the Ab solution and stirred for 20 h at 30 °C. The Ab-Flu conjugate was separated from the unbound dyes by gel permeation chromatography (Sephadex G50). The first fraction containing the Ab-Flu conjugate was collected. A sugar cryoprotectant (5 μ L aliquot of 100 mg/mL solution) was then added to the Ab conjugate solution and lyophilized.

Cy5s-Ab-Flu, DAR(Cy5s) \sim 1.5, and DAR(Flu) \sim 2.4.

Dye Cy5s (1 mg, 4.28 μ mol) was dissolved in DMF (0.25 mL), and then TSTU (5 mg, 16.6 μ mol) and DIPEA (2 μ L) were added. The reaction mixture was stirred for 20 h at 30 °C. Then, Flu-Ab (1 mg) was dissolved in borate buffer pH 8.3 (0.495 mL). An aliquot of preactivated Cy5s (5 μ L) was added to the Flu-Ab solution and stirred for 2 h at 20 °C. The obtained Cy5s-Ab-Flu conjugate was separated by gel permeation chromatography (Sephadex G50). The first fraction containing Cy5s-Ab-Flu was collected, and a sugar cryoprotectant (5 μ L aliquot of 100 mg/mL solution) was added to the Ab conjugate solution and lyophilized.

Cy5s-Ab-Flu-Aza, DAR(Cy5s) \sim 3.0, and DAR(Flu) \sim 1.0. Conjugate Aza-Flu-COOH (0.5 mg, 0.6 μ mol) was dissolved in DMF (0.2 mL), and then TSTU (3 mg, 10 μ mol) and DIPEA (1 μ L) were added to the Aza-Flu-COOH solution. The reaction mixture was stirred for 30 min at 20 °C. Then, Ab-Cy5s (500 μ g) was dissolved in PB pH 7.4 (1.5 mL), and an aliquot of preactivated Aza-Flu-COOH (30 μ L) was added to the Ab-Cy5s solution and stirred for 2 h at 20 °C. The obtained Cy5s-Ab-Flu-Aza conjugate was separated from the unbound Aza-Flu-COOH by gel permeation chromatography (Sephadex G50). The first fraction containing Cy5s-Ab-Flu-Aza was collected, and a sugar cryoprotectant (5 μ L aliquot of 100 mg/mL solution) was added to the Ab conjugate solution and lyophilized.

Spectral Measurements. Absorption spectra were taken on a Jasco V-730 UV/vis spectrophotometer, and the emission spectra were recorded on an Edinburgh Instruments F55 spectrofluorometer. The spectra were measured at RT in a 1 cm quartz microcell for 60 mL at the concentrations of about 1 μ M in 10 mM phosphate buffer pH 7.4 (PB). The emission spectra were measured at the excitation wavelengths λ^* = 480 nm (Flu) and 610 nm (Cy5h, Cy5s).

Dye-to-Antibody Ratio (DAR). DAR for the Ab-Dye (Ab-Cy5h and Ab-Cy5s) conjugates was measured by the spectrophotometric method and calculated according to eq 1⁶⁵

$$\text{DAR} = \frac{A_{\text{max}}(\text{dye}) \times \epsilon_p}{[A_{278} - \alpha \times A_{\text{max}}(\text{dye})] \times \epsilon_d} \quad (1)$$

where $A_{\text{max}}(\text{dye})$ is the absorbance of the Ab-dye conjugate at the dye absorption maximum; A_{278} is the absorbance of the Ab-dye conjugate at 278 nm (absorption maximum of Ab); ϵ_p is the extinction coefficient of Ab; ϵ_d is the extinction coefficient of the dye; and α is the correction factor (the ratio of the A_{278} to $A_{\text{max}}(\text{dye})$ for the dye alone).

Cell Culture. The human breast cancer SKBR3 (HTB-30) cell line was obtained from ATCC (Manassas, VA). Cells were cultured in a McCoy's-5A-based media with penicillin/streptomycin and 10% heat-inactivated fetal bovine serum (FBS). Culture conditions were maintained at 37 °C in a humidified atmosphere containing 5% CO₂.

Microscopy. To monitor the drug release, SKBR3 cells were plated in poly-D-lysine (PDL) coated 0.8 cm²/well Chamber Slides (Thermo Fisher Scientific) at 5,000 cells/well and incubated for 30 min with 10 μ M of an investigated conjugate. After incubation, the cells were washed 3 times with phenol red-free RPMI-1640-based media containing penicillin/streptomycin and 10% FBS and analyzed then by fluorescence microscopy. The imaging experiments were carried out at 37 °C in a humidified atmosphere containing 5% CO₂.

The bright field and fluorescence images were acquired by a Photometrics CoolSNAP HQ2 camera mounted on an Olympus iX81 fluorescent microscope. The microscope was equipped with a 100 W halogen lamp for phase contrast observations and a 120 W metal halide discharge lamp for fluorescence imaging. For the fluorescence imaging, a FITC (green) cube comprising an ET470/40x bandpass excitation filter, ET525/50m bandpass emission filter, and T495lpxr dichroic filter and a Cy5 (red) cube comprising an ET620/60x bandpass excitation filter, ET700/75m bandpass emission filter, and T660lpxr dichroic filter were used.

All the images were taken with the same instrument settings for each channel. The light source intensity was 12%, and the gain was 20.5 dB. Magnification was 100 \times . The exposure time was 1 s for the bright field and green channels and 750 ms for the red channel. The integrated fluorescence intensities (total brightnesses) were quantified for the full images through the integrated density by using the ImageJ software.⁶⁶

Animal Experiments. All animal experiments were carried out in compliance with the Israel Council on Animal Care regulations and were approved by the Animal Care Committee of Ariel University (authorization number IL-179-06-19).

Six-week-old athymic Balb/c male nude mice (Harlan Laboratories, Nes Ziona, Israel) were subcutaneously inoculated on the dorsal left side with SKBR3 (1 \times 10⁶ cells into nu/nu mice, 0.2 mL per mouse), and tumors were allowed to establish over time. When the tumor volume reached a desirable volume (14 days), an investigated conjugate (100 μ L of 0.5 mg/mL solution in PBS) was injected iv (tail), and animals were submitted to the imaging procedure. Each experiment was repeated in triplicate ($n = 3$).

Animal Imaging. Cy5s-Ab-Flu-Aza delivery in tumor was studied on Balb/c male nude mice bearing the SKBR3 tumor model. Imaging was carried out using the multispectral fluorescence *in vivo* imaging system CRi Maestro II. For imaging, acquisition mice were anesthetized by an intraperitoneal injection of chloral hydrate. The imaging was performed after the conjugate administration at intervals from 0 to 30 h (in several experiments up to 6 days) using excitation wavelength 450 nm for Flu and 635 nm for Cy5s. The emission signal of Flu was collected from 500 to 600 nm, and for Cy5s, the emission signal was collected from 675 to 800 nm. The Flu and Cy5s signals were unmixed from the cube file based on the spectra of the nonconjugated fluorophores (Flu-CO₂tBu and Cy5s) and autofluorescence of untreated mice. The data processing was performed by Maestro 3.0 and ImageJ software. Each experiment was carried out in triplicate.

The fluorescence intensity scale bars (in arbitrary units) for the cell microscopy and animal images were obtained by ImageJ software for the 32 bit image mode by using the "Analyze-Tools-Calibration Bar" option. The overlay images were obtained for the RGB image mode by the ImageJ "Image/Color/Merge Channels" option in the 8-bit format.

The ratiometric images were obtained by the “Process–Image Calculator–Divide” option for the 8 bit color and 32 bit grayscale mode, respectively (ImageJ).

■ ASSOCIATED CONTENT

SI Supporting Information

The Supporting Information is available free of charge at <https://pubs.acs.org/doi/10.1021/acs.bioconjchem.1c00205>.

DAR values, spectral data, microscopic and mice images, and LCMS, NMR, and HRMS data (PDF)

■ AUTHOR INFORMATION

Corresponding Author

Leonid Patsenker – Department of Chemical Sciences, the Faculty of Natural Sciences, Ariel University, Ariel 40700, Israel; orcid.org/0000-0002-5541-349X; Email: leonidpa@ariel.ac.il, leonid.patsenker@gmail.com

Authors

Dvir Poplinger – Department of Chemical Sciences, the Faculty of Natural Sciences, Ariel University, Ariel 40700, Israel; orcid.org/0000-0003-2002-9591

Maksym Bokan – Department of Chemical Sciences, the Faculty of Natural Sciences, Ariel University, Ariel 40700, Israel; orcid.org/0000-0001-9882-1760

Arkadi Hesin – Department of Molecular Biology, the Faculty of Natural Sciences, Ariel University, Ariel 40700, Israel; orcid.org/0000-0001-5841-5469

Ebaston Thankarajan – Department of Chemical Sciences, the Faculty of Natural Sciences, Ariel University, Ariel 40700, Israel; orcid.org/0000-0001-5468-0417

Helena Tuchinsky – Department of Molecular Biology, the Faculty of Natural Sciences, Ariel University, Ariel 40700, Israel; orcid.org/0000-0003-1820-4100

Gary Gellerman – Department of Chemical Sciences, the Faculty of Natural Sciences, Ariel University, Ariel 40700, Israel; orcid.org/0000-0002-1336-8707

Complete contact information is available at: <https://pubs.acs.org/doi/10.1021/acs.bioconjchem.1c00205>

Author Contributions

The manuscript was written through contributions of all authors.

Notes

The authors declare no competing financial interest.

■ ACKNOWLEDGMENTS

This research was supported by the Israel Scientific Foundation (ISF), project 810/18. L.P. thanks the Center for Absorption in Science of the Ministry of Immigrant Absorption of Israel for financial support under the KAMEA program. The authors sincerely thank Prof. Michael Sherman for useful discussions and helpful advice, Dr. Galia Luboshits for the fluorescence macroimaging experiments, and Dr. Vered Marks for the NMR measurements (Ariel University).

■ REFERENCES

(1) Dunuweera, S. P., Rajapakse, R. M. S. I., Rajapakshe, R. B. S. D., Wijekoon, S. H. D. P., Nirodha Thilakarathna, M. G. G. S., and Rajapakse, R. M. G. (2019) Review on targeted drug delivery carriers used in nanobiomedical applications. *Curr. Nanosci.* 15 (4), 382–397.

(2) Guo, Y., Huang, L., Zhang, Z., and Fu, D. (2020) Strategies for precise engineering and conjugation of antibody targeted-nanoparticles for cancer therapy. *Curr. Med. Sci.* 40 (3), 463–473.

(3) Cherkasov, V. R., Mochalova, E. N., Babenyshev, A. V., Rozenberg, J. M., Sokolov, I. L., and Nikitin, M. P. (2020) Antibody-directed metal-organic framework nanoparticles for targeted drug delivery. *Acta Biomater.* 103, 223–236.

(4) Alley, S. C., Okeley, N. M., and Senter, P. D. (2010) Antibody-drug conjugates: targeted drug delivery for cancer. *Curr. Opin. Chem. Biol.* 14 (4), 529–537.

(5) Hoppenz, P., Els-Heindl, S., and Beck-Sickinger, A. G. (2020) Peptide-drug conjugates and their targets in advanced cancer therapies. *Front. Chem.* 8, 571.

(6) Yazdi, M. K., Zarrintaj, P., Ghavami, M., Alizadeh, R., and Saeb, M. R. (2020) Protein and peptide-based delivery systems. In *Nanoengineered Biomaterials for Advanced Drug Delivery* (Mozafari, M., Ed.) pp 145–161, Chapter 7, Elsevier, DOI: 10.1016/b978-0-08-102985-5.00007-3.

(7) Majumdar, S., and Siahaan, T. J. (2012) Peptide-mediated targeted drug delivery. *Med. Res. Rev.* 32 (3), 637–658.

(8) Rozovsky, A., Ebaston, T. M., Zaporozhets, A., Bazylevich, A., Tuchinsky, H., Patsenker, L., and Gellerman, G. (2019) Theranostic system for ratiometric fluorescence monitoring of peptide-guided targeted drug delivery. *RSC Adv.* 9 (56), 32656–32664.

(9) Ebaston, T. M., Rozovsky, A., Zaporozhets, A., Bazylevich, A., Tuchinsky, H., Marks, V., Gellerman, G., and Patsenker, L. (2019) Peptide-driven targeted drug delivery system comprising turn-on NIR fluorescent xanthene-cyanine reporter for real time monitoring of drug release. *ChemMedChem* 14 (19), 1727–1734.

(10) Chin, C. F., Yap, S. Q., Li, J., Pastorin, G., and Ang, W. H. (2014) Ratiometric delivery of cisplatin and doxorubicin using tumour-targeting carbon-nanotubes entrapping platinum(IV) prodrugs. *Chem. Sci.* 5 (6), 2265–2270.

(11) Fu, Y., Chen, X., Mou, X., Ren, Z., Li, X., and Han, G. (2016) A dual-color luminescent localized drug delivery system with ratiometric-monitored doxorubicin release functionalities. *ACS Biomater. Sci. Eng.* 2 (4), 652–661.

(12) Yang, K., Zhao, J., Zhang, L., Liu, R., Liang, H., and Zhao, S. (2019) In situ ratiometric fluorescence imaging for tracking targeted delivery and release of anticancer drug in living tumor cells. *ACS Appl. Bio Mater.* 2 (11), 4687–4692.

(13) Hwang, J., Sullivan, M. O., and Kiick, K. L. (2020) Targeted drug delivery via the use of ECM-mimetic materials. *Front. Bioeng. Biotechnol.* 8, 69.

(14) Öztürk-Atar, K., Eroğlu, H., and Çalış, S. (2018) Novel advances in targeted drug delivery. *J. Drug Target.* 26 (8), 633–642.

(15) Pattni, B. S., and Torchilin, V. P. (2015) Targeted drug delivery systems: strategies and challenges. In *Targeted Drug Delivery: Concepts and Design. Advances in Delivery Science and Technology* (Devarajan, P., and Jain, S., Eds.) pp 3–38, Chapter 1, Springer, Cham, DOI: 10.1007/978-3-319-11355-5_1.

(16) Patsenker, L., and Gellerman, G. (2020) Fluorescent reporters for drug delivery monitoring. *Isr. J. Chem.* 60 (5–6), 504–518.

(17) Zheng, F., Xiong, W., Sun, S., Zhang, P., and Zhu, J. J. (2019) Recent advances in drug release monitoring. *Nanophotonics* 8 (3), 391–413.

(18) Ash, C., Dubec, M., Donne, K., and Bashford, T. (2017) Effect of wavelength and beam width on penetration in light-tissue interaction using computational methods. *Lasers Med. Sci.* 32 (8), 1909–1918.

(19) Badugu, R., Lakowicz, J. R., and Geddes, C. D. (2005) A glucose-sensing contact lens: From bench top to patient. *Curr. Opin. Biotechnol.* 16 (1), 100–107.

(20) Shi, L., Yan, C., Guo, Z., Chi, W., Wei, J., Liu, W., Liu, X., Tian, H., and Zhu De, W. H. (2020) Novo strategy with engineering anti-kasha/kasha fluorophores enables reliable ratiometric quantification of biomolecules. *Nat. Commun.* 11 (1), 793.

- (21) Lee, M. H., Kim, J. S., and Sessler, J. L. (2015) Small molecule-based ratiometric fluorescence probes for cations, anions, and biomolecules. *Chem. Soc. Rev.* 44 (13), 4185–4191.
- (22) Huang, X., Song, J., Yung, B. C., Huang, X., Xiong, Y., and Chen, X. (2018) Ratiometric optical nanoprobe enable accurate molecular detection and imaging. *Chem. Soc. Rev.* 47 (8), 2873–2920.
- (23) Duan, X., Li, N., Wang, G., and Su, X. (2020) High sensitive ratiometric fluorescence analysis of trypsin and dithiothreitol based on WS2 QDs. *Talanta* 219, 121171.
- (24) Gui, R., Jin, H., Bu, X., Fu, Y., Wang, Z., and Liu, Q. (2019) Recent advances in dual-emission ratiometric fluorescence probes for chemo/biosensing and bioimaging of biomarkers. *Coord. Chem. Rev.* 383, 82–103.
- (25) Chen, C., Tian, R., Zeng, Y., Chu, C., and Liu, G. (2020) Activatable fluorescence probes for “Turn-On” and ratiometric biosensing and bioimaging: From NIR-I to NIR-II. *Bioconjugate Chem.* 31 (2), 276–292.
- (26) Kong, X., Dong, B., Song, X., Wang, C., Zhang, N., and Lin, W. (2018) Dual turn-on fluorescence signal-based controlled release system for real-time monitoring of drug release dynamics in living cells and tumor tissues. *Theranostics* 8 (3), 800–811.
- (27) Zhang, Y., Wei, C., Lv, F., and Liu, T. (2018) Real-Time imaging tracking of a dual-fluorescent drug delivery system based on doxorubicin-loaded globin-polyethylenimine nanoparticles for visible tumor therapy. *Colloids Surf., B* 170, 163–171.
- (28) Porubský, M., Gurská, S., Stanková, J., Hajdúch, M., Džubák, P., and Hlaváč, J. (2019) Amino-BODIPY as the ratiometric fluorescent sensor for monitoring drug release or “Power Supply” selector for molecular electronics. *RSC Adv.* 9 (43), 25075–25083.
- (29) Ye, M., Wang, X., Tang, J., Guo, Z., Shen, Y., Tian, H., and Zhu, W. H. (2016) Dual-channel NIR activatable theranostic prodrug for: In vivo spatiotemporal tracking thiol-triggered chemotherapy. *Chem. Sci.* 7 (8), 4958–4965.
- (30) Choi, P. J., Park, T. I. H., Cooper, E., Dragunow, M., Denny, W. A., and Jose, J. (2020) Heptamethine cyanine dye mediated drug delivery: Hype or hope. *Bioconjugate Chem.* 31 (7), 1724–1739.
- (31) Bouchaala, R., Mercier, L., Andreiuk, B., Mély, Y., Vandamme, T., Anton, N., Goetz, J. G., and Klymchenko, A. S. (2016) Integrity of lipid nanocarriers in bloodstream and tumor quantified by near-infrared ratiometric FRET imaging in living mice. *J. Controlled Release* 236, 57–67.
- (32) Trier, N. H., and Houen, G. (2020) Antibodies as diagnostic targets and as reagents for diagnostics. *Antibodies* 9 (2), 15.
- (33) Van Elslande, J., Houben, E., Depypere, M., Brackenier, A., Desmet, S., André, E., Van Ranst, M., Lagrou, K., and Vermeersch, P. (2020) Diagnostic performance of seven rapid IgG/IgM antibody tests and the euroimmuno IgA/IgG ELISA in COVID-19 patients. *Clin. Microbiol. Infect.* 26 (8), 1082–1087.
- (34) Bazylevich, A., Patsenker, L. D., and Gellerman, G. (2017) Exploiting fluorescein based drug conjugates for fluorescent monitoring in drug delivery. *Dyes Pigm.* 139, 460–472.
- (35) Cline, S. D., Macdonald, T. L., and Osheroff, N. (1997) Azatoxin is a mechanistic hybrid of the topoisomerase II-targeted anticancer drugs etoposide and ellipticine. *Biochemistry* 36 (42), 13095–13101.
- (36) Li, C., Xiong, W., Liu, X., Xiao, W., Guo, Y., Tan, J., and Li, Y. (2019) Hypomethylation at Non-CpG/CpG sites in the promoter of HIF-1 α gene combined with enhanced H3K9Ac modification contribute to maintain higher HIF-1 α expression in breast cancer. *Oncogenesis* 8 (4), 26.
- (37) Lewis Phillips, G. D., Li, G., Dugger, D. L., Crocker, L. M., Parsons, K. L., Mai, E., Blättler, W. A., Lambert, J. M., Chari, R. V. J., Lutz, R. J., et al. (2008) Targeting HER2-positive breast cancer with trastuzumab-DM1, an antibody-cytotoxic drug conjugate. *Cancer Res.* 68 (22), 9280–9290.
- (38) Holliday, D. L., and Speirs, V. (2011) Choosing the right cell line for breast cancer research. *Breast Cancer Res.* 13 (4), 215.
- (39) Gunturu, K. S., Woo, Y., Beaubier, N., Remotti, H. E., and Saif, M. W. (2013) Gastric cancer and trastuzumab: first biologic therapy in gastric cancer. *Ther. Adv. Med. Oncol.* 5 (2), 143–151.
- (40) Tosi, F., Sartore-Bianchi, A., Lonardi, S., Amatu, A., Leone, F., Ghezzi, S., Martino, C., Bencardino, K., Bonazzina, E., Bergamo, F., et al. (2020) Long-term clinical outcome of trastuzumab and lapatinib for her2-positive metastatic colorectal cancer. *Clin. Colorectal Cancer* 19 (4), 256–262.e2.
- (41) Azzoli, C. G., Krug, L. M., Miller, V. A., Kris, M. G., and Mass, R. (2002) Trastuzumab in the treatment of non-small cell lung cancer. *Semin. Oncol.* 29 (1 Suppl 4), 59–65.
- (42) Cui, X., and Iwenofu, O. H. (2020) HER2-positive metastatic melanoma: a cautionary tale! *Appl. Immunohistochem Mol. Morphol.* 28 (8), e73–e75.
- (43) Chevallier, P., Robillard, N., Charbonnier, A., Raffoux, E., Maury, S., Carras, S., Chabrot, C., Fohrer, C., Bernard, M., Blade, J. S., et al. (2012) Trastuzumab for treatment of refractory/relapsed HER2-positive adult B-ALL: results of a phase 2 GRAALL study. *Blood* 119 (11), 2474–2477.
- (44) Haen, S. P., Schmiedel, B. J., Rothfelder, K., Schmied, B. J., Dang, T. M., Mirza, N., Möhle, R., Kanz, L., Vogel, W., and Salih, H. R. (2016) Prognostic relevance of HER2/neu in acute lymphoblastic leukemia and induction of NK cell reactivity against primary ALL blasts by trastuzumab. *Oncotarget* 7 (11), 13013–13030.
- (45) Solary, E., Leteurtre, F., Paull, K. D., Scudiero, D., Hamel, E., and Pommier, Y. (1993) Dual inhibition of topoisomerase II and tubulin polymerization by azatoxin, a novel cytotoxic agent. *Biochem. Pharmacol.* 45 (12), 2449–2456.
- (46) Pöplinger, D., Bazylevich, A., Bokan, M., Gellerman, G., and Patsenker, L. (2021) Dual-dye systems comprising activatable fluorescein dye and hydrophobic or hydrophilic Cy5 reference fluorophore for ratiometric drug delivery monitoring. *J. Photochem. Photobiol., A* 408, 113113.
- (47) Markova, L. I., Fedyunyayeva, I. A., Povrozin, Ye. A., Semenova, O. M., Khabuseva, S. U., Terpetschnig, E. A., and Patsenker, L. D. (2013) Water soluble indodicarbocyanine dyes based on 2,3-dimethyl-3-(4-sulfobutyl)-3H-indole-5-sulfonic acid. *Dyes Pigm.* 96 (2), 535–546.
- (48) Hahn, C. D., Riener, C. K., and Gruber, H. J. (2001) Labeling of antibodies with Cy3-, Cy3.5-, Cy5-, and Cy5.5-monofunctional dyes at defined dye/protein ratios. *Single Mol.* 2, 149–149.
- (49) Harlow, E., and Lane, D. (1999) *Using Antibodies, A Laboratory Manual*, Cold Spring Harbor Laboratory Press, New York.
- (50) 38371 Atto 488 Protein Labeling Kit, Sigma-Aldrich. <https://www.sigmaaldrich.com/content/dam/sigma-aldrich/docs/Sigma/Datasheet/6/38371dat.pdf> (accessed 2021-06-08).
- (51) Markova, L. I., Terpetschnig, E. A., and Patsenker, L. D. (2013) Comparison of a series of hydrophilic squaraine and cyanine dyes for use as biological labels. *Dyes Pigm.* 99, 561–570.
- (52) West, W., and Pearce, S. (1965) The dimeric state of cyanine dyes. *J. Phys. Chem.* 69, 1894–1903.
- (53) Andreiuk, B., Reisch, A., Bernhardt, E., and Klymchenko, A. S. (2019) Fighting aggregation-caused quenching and leakage of dyes in fluorescent polymer nanoparticles: Universal role of counterion. *Chem. - Asian J.* 14 (6), 836–846.
- (54) Markova, L. I., Terpetschnig, E. A., and Patsenker, L. D. (2013) Comparison of a series of hydrophilic squaraine and cyanine dyes for use as biological labels. *Dyes Pigm.* 99 (3), 561–570.
- (55) Jasinski, D. L., Yin, H., Li, Z., and Guo, P. (2018) Hydrophobic effect from conjugated chemicals or drugs on in vivo biodistribution of RNA nanoparticles. *Hum. Gene Ther.* 29 (1), 77–86.
- (56) Hardiansyah, A., Yang, M. C., Liu, T. Y., Kuo, C. Y., Huang, L. Y., and Chan, T. Y. (2017) Hydrophobic drug-loaded PEGylated magnetic liposomes for drug-controlled release. *Nanoscale Res. Lett.* 12, 355.
- (57) Achilefu, S., Jimenez, H. N., Dorshow, R. B., Bugaj, J. E., Webb, E. G., Wilhelm, R. R., Rajagopalan, R., Johler, J., and Erion, J. L. (2002) Synthesis, in vitro receptor binding, and in vivo evaluation of

fluorescein and carbocyanine peptide-based optical contrast agents. *J. Med. Chem.* 45 (10), 2003–2015.

(58) van Dam, G. M., Themelis, G., Crane, L. M., Harlaar, N. J., Pleijhuis, R. G., Kelder, W., Sarantopoulos, A., de Jong, J. S., Arts, H. J., van der Zee, A. G., et al. (2011) Intraoperative tumor-specific fluorescence imaging in ovarian cancer by folate receptor- α targeting: first in-human results. *Nat. Med.* 17 (10), 1315–1319.

(59) Troy, T., Jekic-McMullen, D., Sambucetti, L., and Rice, B. (2004) Quantitative comparison of the sensitivity of detection of fluorescent and bioluminescent reporters in animal models. *Mol. Imaging* 3 (1), 9–23.

(60) Wirth, D., Byrd, B., Meng, B., Strawbridge, R. R., Samkoe, K. S., and Davis, S. C. (2021) Hyperspectral imaging and spectral unmixing for improving whole-body fluorescence cryo-imaging. *Biomed. Opt. Express* 12 (1), 395–408.

(61) Stanta, G., and Bonin, S. (2018) Overview on clinical relevance of intra-tumor heterogeneity. *Front. Med.* 5, 85.

(62) Denison, T. A., and Bae, Y. H. (2012) Tumor heterogeneity and its implication for drug delivery. *J. Controlled Release* 164 (2), 187–191.

(63) Junttila, M. R., and de Sauvage, F. J. (2013) Influence of tumour micro-environment heterogeneity on therapeutic response. *Nature* 501 (7467), 346–354.

(64) Pande, G., Das, M. R., Joshi, D. S., and Sundaram, K. (1986) Isolation and characterization of the two subpopulations of cells with different lethality from Zajdela ascitic hepatoma. *Cancer Res.* 46 (4), 1673–1678.

(65) Nath, N., Godat, B., and Urh, M. (2016) Antibody labeling with fluorescent dyes using magnetic Protein A and Protein G beads. *J. Visualized Exp.* 115, No. e54545.

(66) Rasband, W. S. (1997-2018) *ImageJ*, U.S. National Institutes of Health, Bethesda, Maryland, USA. <https://imagej.nih.gov/ij/> (accessed 2021-06-08).